Study of cell distribution functions of the three-dimensional Ising model

K. Kaski
Physics Department, Temple University, Philadelphia, Pennsylvania 19122

K. Binder
Institut für Festkörperforschung der Kernforschungsanlage Jülich, Postfach 1913, D-5170 Jülich 1, West Germany

J. D. Gunton
Physics Department, Temple University, Philadelphia, Pennsylvania 19122
(Received 7 November 1983)

The single and joint distribution functions of the nearest-neighbor cell magnetization of the three-dimensional Ising model have been studied by Monte Carlo methods. Near the critical point, both distribution functions tend, for large L, towards scaled universal forms. Estimates of the order parameter and susceptibility are obtained from the distribution functions. The critical temperature is estimated by a method independent of the estimate of the critical exponents. The critical exponent ν is obtained with the use of finite-size scaling arguments. The joint distribution function shows a double-well structure for $T < T_c$ and can be represented by a coarse-grained effective Hamiltonian of two cell variables. We have determined the dependence of this functional on the coarse-graining cell size for several temperatures. In particular, we have calculated the dependence of the "spinodal curve" on the (scaled) coarse-graining size. The relevance of this work to the kinetics of first-order phase transitions is also discussed.

I. INTRODUCTION

It is well known that the concept of dividing a system into "cells" or "blocks" of finite linear dimension L has useful applications in many statistical mechanical problems. This concept has been applied, for example, to understand phase coexistence in the van der Waals fluid[1] and to derive scaling laws between critical exponents.[2] As well, for a large class of problems the understanding of the "coarse-grained" Helmholtz free-energy functional is fundamentally important.[3] Such problems include wetting,[4] the surface tension and interface profile of gas-liquid and liquid-liquid interfaces,[5,6] and nucleation and spinodal decomposition processes.[7,8] Also the coarse-grained free-energy functional provides a starting point for the renormalization-group theory of critical phenomena.[9–12]

A quantity which has played an important conceptual role in the theory of metastable and unstable states is the so-called spinoidal curve. This can be given a precise definition within the context of mean-field or van der Waals type theories valid for systems with infinitely long-range forces. Recall that in the van der Waals picture, there is a "van der Waals" loop which does not describe thermodynamic equilibrium states. Rather, the outer portions of the loop (for which the order-parameter isothermal susceptibility is positive) describe metastable states. The inner portion of the loop (for which the susceptibility is negative) describes unstable states. The two points at which the inverse susceptibility vanishes (for fixed $T < T_c$) are known as spinodal points and in mean-field theories provide a sharp distinction between metastable and unstable states. The locus of these points as a function of temperature defines the classical spinodal curve.

For systems with finite-range forces, however, the situation is much more subtle. One can, in fact, imagine giving at least two different definitions of a "spinodal curve." The first would be the analog of the van der Waals picture. Namely, consider the problem of analytically continuing the equilibrium free energy of a stable phase into the metastable part of the two-phase region. Since it is reasonably well established that there is an essential singularity in this free energy at any point on the coexistence curve below T_c, the analytic continuation consists of a real and an imaginary part. This real part $\tilde{f}(s)$ is schematically indicated in Fig. 1 by the dashed lines. The interpretation of this real part is that it describes the *equilibrium* properties of the metastable state. That is, it would describe such quantities as the susceptibility and specific heat in experimental measurements of a metastable state on a time scale during which the state has not begun to decay. If this dashed line has a unique continuation the extrapolated value of the measured susceptibility would appear to diverge at some point (for fixed T). This could provide one definition of a "pseudo-spinodal" point.[13] However, in the dynamical theory of unstable and metastable states, the fundamental quantity which occurs in the equations of motion is the coarse-grained Helmholtz free-energy functional (Ginzburg-Landau Hamiltonian) mentioned above. This contains in addition to the usual gradient term a free-energy density $f(s)$ which has the form of a double-well potential for $T < T_c$. This is shown in Fig. 1. It is this double-well potential (whose shape depends on the particular coarse-graining size chosen in the theory) which describes the *nonequilibrium* properties of the system. Thus there are two quite different free ener-

 ©1984 The American Physical Society

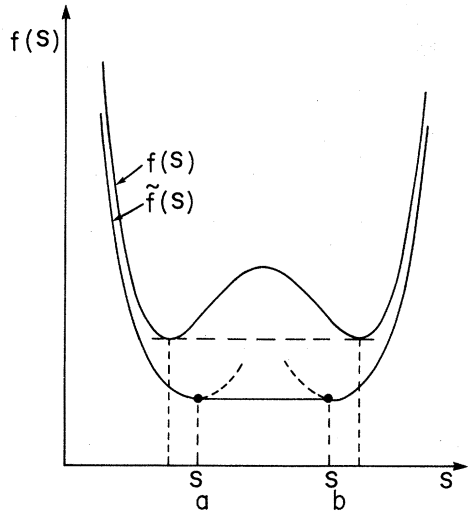

FIG. 1. Schematic graph of the coarse-grained free energy $f(s)$ and the corresponding equilibrium free energy $\tilde{f}(s)$. The dashed sections denote the analytic continuation of $\tilde{f}(s)$ into the metastable region.

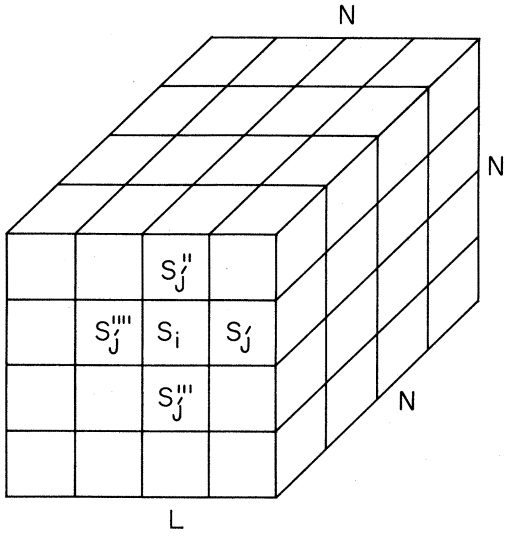

FIG. 2. Division of $N\times N\times N$ system into cells of linear dimension L. s_i represents the degrees of freedom of the ith cell. Some cells which are nearest neighbors of the ith cell are shown.

gies, the coarse grained $f(s)$ and the analytic continuation of the equilibrium free energy $\tilde{f}(s)$.

Since it is the former quantity $f(s)$ which enters the dynamical equations of motion, it is the relevant quantity for any dynamical theory of spinodal decomposition, etc. As a consequence one can use $f(s)$ (which depends on the coarse-graining size L) to define a so-called "coarse-grained" spinodal curve, for which $\partial^2 f/\partial s^2=0$. Since $f(s)$ depends on L, the coarse-grained spinodal curve will also depend on L. That is, there is no unique coarse-grained spinodal curve. One major goal of this paper is to demonstrate this rather obvious fact (which is often a source of confusion in the literature). We do this by an explicit calculation of an effective Hamiltonian which is analogous (but not identical) to the coarse-grained Helmholtz functional. From this effective Hamiltonian we can define an effective coarse-grained spinodal curve which we show has all the properties to be expected for the coarse-grained spinodal curve obtained from the Helmholtz free-energy functional.

For the dynamical theory of spinodal decomposition it would obviously be useful to evaluate this free-energy functional $f(s)$ starting from some initial microscopic model Hamiltonian. It would be particularly useful for a coarse-graining cell size whose linear dimension L is of the order of the correlation length ξ, since this is the scale on which the dynamics of phase separation is treated. Although we are unable to evaluate $f(s)$ in this present study, we outline now one way of determining $f(s)$ in principle. Our model Hamiltonian is the three-dimensional Ising model in zero magnetic field:

$$\mathcal{H}=-J\sum_{l,l'} S_l S_{l'} \,. \tag{1.1}$$

We proceed as previously done[12,14,15] by dividing the $N\times N\times N$ system into cells of linear dimension L, as shown in Fig. 2. The magnetization per spin of cell i is defined as

$$s_i=L^{-d}\sum_{l\in i} S_l \,, \tag{1.2}$$

where the sum is over all lattice sites l in the cell i, and $S_l=\pm 1$. It is assumed that the Boltzmann factor $Z^{-1}\exp(-\mathcal{H}/k_BT)$ with the given constraint, Eq. (1.2), can be written in terms of the discrete coarse-grained Ginzburg-Landau (GL) Hamiltonian

$$P_L(\{s_i\})=Z^{-1}\exp[-\mathcal{H}_{\rm GL}(\{s_i\})] \,, \tag{1.3}$$

where

$$\mathcal{H}_{\rm GL}(\{s_i\})=\sum_i (\tilde{h}_L s_i-\tilde{r}_L s_i^2+\tilde{u}_L s_i^4+\tilde{v}_L s_i^6+\cdots) + \sum_{\langle i,j\rangle} \tilde{c}_L (s_i-s_j)^2+\cdots \,. \tag{1.4}$$

The factor $(k_BT)^{-1}$ is absorbed in the Ginzburg-Landau Hamiltonian, Z denotes the partition function, and $\langle i,j\rangle$ denotes the sum over nearest-neighbor cells (see Fig. 2). In order that the coefficients in (1.4), $\tilde{r}_L,\tilde{u}_L,\ldots,\tilde{c}_L,\ldots$, depend on temperature and other external parameters in a nonsingular way, it is crucial that $L\ll\xi$. Close enough to T_c where ξ is arbitrarily large one can choose $L\gg 1$ (measured in units of the lattice spacing) and then proceed by replacing (1.4) by a continuum approximation. The polynomial in s in Eq. (1.4) would then yield $f(s)$.

Although the relationship between Eqs. (1.1) and (1.4) is of crucial conceptual importance, it is hardly ever carried out explicitly. As a consequence the resulting theories of first- and second-order phase transitions can only predict the universal properties of the system. Thus information on nonuniversal properties such as on interaction parameter ratios, lattice spacing, e.g., is lost. While it is essentially impossible to perform this coarse graining exactly, it is possible to obtain numerical results by Monte Carlo methods, sampling the distribution function $P_L(\{s_i\})$. Sampling the total distribution function is obviously ex-

tremely difficult. Therefore, in this paper we have studied the two simplest distribution functions

$$P_L(s_i,s_j)=\int \prod_{\substack{l\neq i\\ l\neq j\\ \langle i,j\rangle}} ds_l P_L(\{s_l\}) \tag{1.5}$$

and

$$P_L(s_i)=\int ds_j P_L(s_i,s_j)\ . \tag{1.6}$$

In Eq. (1.5) i and j denote nearest-neighbor cells. Thus $P_L(s_i,s_j)$ has a contribution related to a "gradient" parameter c_L in the ansatz (1.4).

The organization of this paper is as follows: In Sec. II we discuss the properties of the distribution functions for $L \ll \xi$ and $L \gg \xi$. The properties of the single distribution function are discussed very briefly, since a detailed discussion can be found in Ref. 12. A Ginzburg-Landau—type parametrization of $P_L(s_i)$ and $P_L(s_i,s_j)$ is discussed. In Sec. III we present the numerical results of our Monte Carlo study. At many points the previous analysis by one of us[12] is repeated, since in this work there was a small programming error resulting in the sampling of a slightly different distribution, as noted in Ref. 12. Only very small numerical deviations from the previous results were found. In Sec. IV we perform the Ginzburg-Landau—type parametrization of $P_L(s_i,s_j)$ and $P_L(s_i)$ and compare our results with field-theoretic calculations. The size dependence of a coarse-grained "spinodal" curve will be discussed.

II. GENERAL PROPERTIES OF THE CELL DISTRIBUTION FUNCTIONS

A. Single cell distribution function $P_L(s)$

Since the single cell distribution function has been discussed earlier in detail by one of us,[12] we will present here only a short summary of the results which are relevant to this study. For zero magnetic field the distribution function $P_L(s)$ is symmetric, i.e., $P_L(s)=P_L(-s)$. This holds as such for $T>T_c$. Below T_c, where a spontaneous magnetization (with two different values $\pm M$) appears in the thermodynamic limit, the symmetrization $P_L^{(s)}(s)=[P_L(s)+P_L(-s)]/2$ has to be implemented to regain the above symmetry.

For the scaling analysis we need moments and cumulants of the cell distribution function. The kth moment is defined as follows:

$$\langle s^k\rangle_L=\int ds\, s^k P_L(s)\ . \tag{2.1}$$

The first cumulant (which we will use) is

$$U_L=1-\frac{\langle s^4\rangle}{3(\langle s^2\rangle_L)^2}\ . \tag{2.2}$$

It was shown[12] that for $T>T_c$ all the cumulants vanish as $L\to\infty$, so that $P_L(s)$ is a Gaussian distribution function. This is also rigorously proven using the central limit theorem of probability theory.[16] For $T<T_c$ the situation is much more complicated since the symmetrized distribution function shows a double-peak structure. It is plausible to use two displaced Gaussian distribution functions to represent $P_L(s)$ for $T<T_c$ in the limit $L\to\infty$. As far as we know no theorems exist that such a two Gaussian representation is correct. This representation could be reasonable only near the peaks of the distribution, but in the regime $-\langle\,|s|\,\rangle_L \ll s \ll \langle\,|s|\,\rangle_L$, $P_L(s)$ is dominated by configurations which correspond to two-phase coexistence within the cell L^d. Above T_c the second moment of the cell distribution function is related to the susceptibility χ_L for a cell of linear size L as follows:

$$L^{-d}k_BT\chi_L=L^{-2d}\sum_{i,j\in\text{cell}}\langle S_iS_j\rangle_T$$
$$=\langle s^2\rangle_L,\quad T>T_c\ . \tag{2.3}$$

χ_L is a good estimate of the susceptibility χ of the infinite system in the case that $L\gg\xi$ where ξ is the order-parameter correlation length. Below T_c the cell susceptibility is defined as

$$k_BT\chi_L=L^d(\langle s^2\rangle_L-\langle\,|s|\,\rangle_L^2)\to k_BT\chi,\quad T<T_c \tag{2.4}$$

where

$$\langle\,|s|\,\rangle_L=\left\langle\left|\sum_{i\in\text{cell}}S_i\right|\right\rangle_T$$

is the cell magnetization.

The distribution function $P_L(s)$ in the vicinity of the critical-point scales as

$$P_L(s)=L^{\beta/\nu}aC_0^{-1}\tilde{P}(asL^{\beta/\nu},\xi L^{-1})\ , \tag{2.5}$$

where $\tilde{P}(z,z')$ is a universal scaling function, a is a constant, $C_0=\int_{-\infty}^{+\infty}dz\,\tilde{P}(z,\infty)$ is a universal constant, and β and ν are the critical exponents for the spontaneous magnetization M and correlation length ξ, respectively. Thus one can write the moments (cumulants) in the scaling form

$$\langle s^k\rangle_L=L^{-k\beta/\nu}(a^kC_0)^{-1}f_k(\xi L^{-1})\ , \tag{2.6}$$

where $f_k(\xi L^{-1})$ is a universal function.

B. Joint nearest-neighbor cell distribution function $P_L(s_1,s_2)$

Now we consider the joint distribution function $P_L(s_1,s_2)$ for nearest-neighbor cells (see Fig. 2). As mentioned in the Introduction the single cell distribution function $P_L(s)$ is obtained from the joint distribution function by integrating out one of the cell spin degrees of freedom. The symmetry properties of $P_L(s_1,s_2)$ are the same as for $P_L(s)$, i.e.,

$$P_L(s_1,s_2)=P_L(-s_1,-s_2)\ . \tag{2.7}$$

In addition to this spin-flip symmetry one also has

$$P_L(s_1,s_2)=P_L(s_2,s_1)\ . \tag{2.8}$$

Below T_c these properties are valid for the symmetrized cell distribution function

$$P_L^{(s)}(s_1,s_2)=\tfrac{1}{4}[P_L(s_1,s_2)+P_L(s_2,s_1)$$
$$+P_L(-s_1,-s_2)+P_L(-s_2,-s_1)] . \quad (2.9)$$

From now on we will suppress our notation $P_L^{(s)}(s_1,s_2)\to P_L(s_1,s_2)$ to mean the symmetrized distribution function.

As discussed above the full distribution function $P_L(\{s_i\})$ above T_c for large linear system size L can be expressed by a multivariate Gaussian, having its maximum at $\{s_i\}=\{0\}$.[16] For the joint distribution function this naturally means that $P_L(s_1,s_2)$ can be written as a bivariate Gaussian

$$P_L(s_1,s_2)=[2\pi\langle s^2\rangle_L(1-\rho^2)^{1/2}]^{-1}\exp\{-[2(1-\rho^2)\langle s^2\rangle_L]^{-1}(s_1^2-2\rho s_1s_2+s_2^2)\} , \quad (2.10)$$

where $\rho=\langle s_1s_2\rangle_L/\langle s^2\rangle_L$ is a measure of the correlations between cell spins s_1 and s_2. $\langle s_1s_2\rangle_L$ refers to the first "cross" moment of the joint distribution function. The general (k,l)th cross moments are defined as

$$\langle s_1^k s_2^l\rangle=\int\int ds_1ds_2s_1^ks_2^lP_L(s_1,s_2) . \quad (2.11)$$

The first cross moment describes long-range correlations as does χ_L in Eq. (2.3). However,

$$\langle s_1s_2\rangle=L^{-2}\sum_{\substack{\alpha\in 1\\ \beta\in 2}}\langle S_\alpha S_\beta\rangle_T$$

does not approach the true susceptibility for $L\to\infty$, since the sum is weighted differently from that in Eq. (2.3) for $\langle s^2\rangle_L$. Hence the amplitude of $\langle s_1s_2\rangle_L$ must differ from that of $\langle s^2\rangle_L$. We do expect, however, the qualitative behavior of $\langle s_1s_2\rangle_L$ to be the same as that of $\langle s^2\rangle_L$ in the critical region. Below T_c it would be plausible to represent $P_L(s_1,s_2)$ by the sum of two displaced bivariate Gaussians, but this would at most be valid only in the neighborhood of the peaks $s_{1\,\max}=s_{2\,\max}$ (as in the case of the single cell distribution function).

Now we will consider the scaling behavior of the joint cell distribution function. We assume that for $T\to T_c$ and $L\to\infty$

$$P_L(s_1,s_2)=L^{x'}\hat{P}_2\tilde{P}_2(bs_1L^{y'},bs_2L^{y'},\xi/L) , \quad (2.12)$$

where we have taken into account the symmetry properties (2.7) and (2.8). It is easy to show that $x'=2y'$ and $\hat{P}_2=b^2/C_1$ where

$$C_1=\int\int\tilde{P}_2(z,z',\infty)dz\,dz'$$

is a universal constant. To show this we have used the normalization

$$\int\int ds_1ds_2P_L(s_1,s_2)=1 .$$

We have used Eq. (1.6) to relate the constants of the scaled joint distribution function with those appearing in the scaled single distribution function, Eq. (2.5). Thus we can now rewrite the scaling hypothesis as follows:

$$P_L(s_1,s_2)=L^{2\beta/\nu}a^2/C_0\tilde{P}_2(as_1L^{\beta/\nu},as_2L^{\beta/\nu},\xi/L) . \quad (2.13)$$

The scaling form for the "cross" moments now reads

$$\langle s_1^k s_2^l\rangle_L=L^{-2(k+l)\beta/\nu}(a^{(k+l)}C_0)^{-1}f_{k+l}(\xi/L) , \quad (2.14)$$

where f_{k+l} is the universal function related to the (k,l)th "cross" moment.

Next we will discuss the parametrization of the single and joint cell distribution functions in terms of a double-well potential and a gradient term. In the Introduction it was mentioned that the total distribution function $P_L(\{s_i\})$ could be parametrized in terms of the Ginzburg-Landau Hamiltonian. Instead of the most general form, Eqs. (1.3) and (1.4), we have taken the following s^4 *Ansatz* with a nearest-neighbor cell gradient term:

$$\mathcal{H}_{\rm GL}(\{s_i\})=\sum_i(-\tilde{r}_Ls_i^2+\tilde{u}_Ls_i^4)+\sum_{\langle i,j\rangle}\tilde{c}_L(s_i-s_j)^2$$
$$=\sum_i V_L(s_i)+\sum_{\langle i,j\rangle}\tilde{c}_L(s_i-s_j)^2 . \quad (2.15)$$

We will assume that a similar parametrization can be used for the joint cell distribution function so that

$$P_L(s_1,s_2)=Z^{-1}B(c_Ls_1,c_Ls_2)\exp[-V_L(s_1)-V_L(s_2)-\tilde{c}_L(s_1-s_2)^2] , \quad (2.16)$$

where

$$B_L(c_Ls_1,c_Ls_2)=\int ds_3\cdots ds_N\exp\left[-\sum_{i=3}^N V_L(s_i)-\sum_{\substack{\langle i,j\rangle\\ i,j\neq 1,2}}\tilde{c}_L(s_i-s_2)^2-\sum_{i\neq 2}^N\tilde{c}_L(s_i-s_1)^2-\sum_{j=2}^N\tilde{c}_L(s_j-s_2)^2\right] .$$

Thus we parametrize $P_L(s_1,s_2)$ as

$$P_L(s_1,s_2)=(Z')^{-1}\exp[+r_L(s_1^2+s_2^2)-u_L(s_1^4+s_2^4)-c_L(s_1-s_2)^2] , \quad (2.17)$$

where the parameters r_L, u_L, and c_L have changed from their original values, in Eq. (2.15), due to the gradient parameter c_L. It should be mentioned, however, that if $\tilde{c}_L$ is vanishingly small, $r_L\to\tilde{r}_L$ and $u_L\to\tilde{u}_L$. How good a parametrization (2.17) is depends obviously on the strength of the gradient term. Rigorously speaking this parametrization is arbitrary. However, we will how that our numerical results are consistent with this parametrization. A similar procedure can be carried out for the single distribution function

$$P_L(s)=(Z'')^{-1}\exp(+r_L's^2-u_L's^4)\ . \tag{2.18}$$

We will use these parametrizations to analyze our Monte Carlo data. The effect of the gradient term c_L on the parameters r_L and u_L can be tested by comparing these parameters as obtained from Eqs. (2.17) and (2.18), respectively. Also the double-well structure of V_L will be compared with those obtained from field-theoretic *Ansätze* and estimates.

III. MONTE CARLO RESULTS AND ANALYSIS

We have studied a simple cubic $24\times24\times24$ Ising lattice with the use of standard Monte Carlo techniques. The linear sizes of the cells studied were $L=2$, 3, 4, 6, and 8. A satisfactory accuracy for $P_L(s)$ and $P_L(s_1,s_2)$ was obtained when effectively about 2.10^4 MCS/spin (Monte Carlo steps per spin) were performed. Near the critical point the number of MCS/spin was doubled.

In Fig. 3 we show some of the "raw data" of the simulation for $P_L(s_1,s_2)$ below and above T_c for different cell sizes L^3. The peaks increase in height with increasing L, as expected. Below T_c the peaks in $P_L(s_1,s_2)$ and $P_L(s)$ are asymmetric, reflecting the expected structure due to the two-phase coexistence for $s<s_{\max}$. It should also be mentioned that cross sections of the $P_L(s_1,s_2)$ peaks do not show the ellipsoidal shapes one would expect if the Gaussian description were correct. It is clear that the s^{2n} terms, $n=2,3,\ldots$, play an important role in determining the peaks. We will use these features later on when parametrizing the joint distribution function in order to give estimates for the double-well and gradient parameters [see Eqs. (2.17) and (2.18)].

In Fig. 4 we have shown estimates of the magnetization as obtained from the absolute first moment $\langle\,|s|\,\rangle_L$, the square root of the second moment $(\langle s^2\rangle_L)^{1/2}$, and the

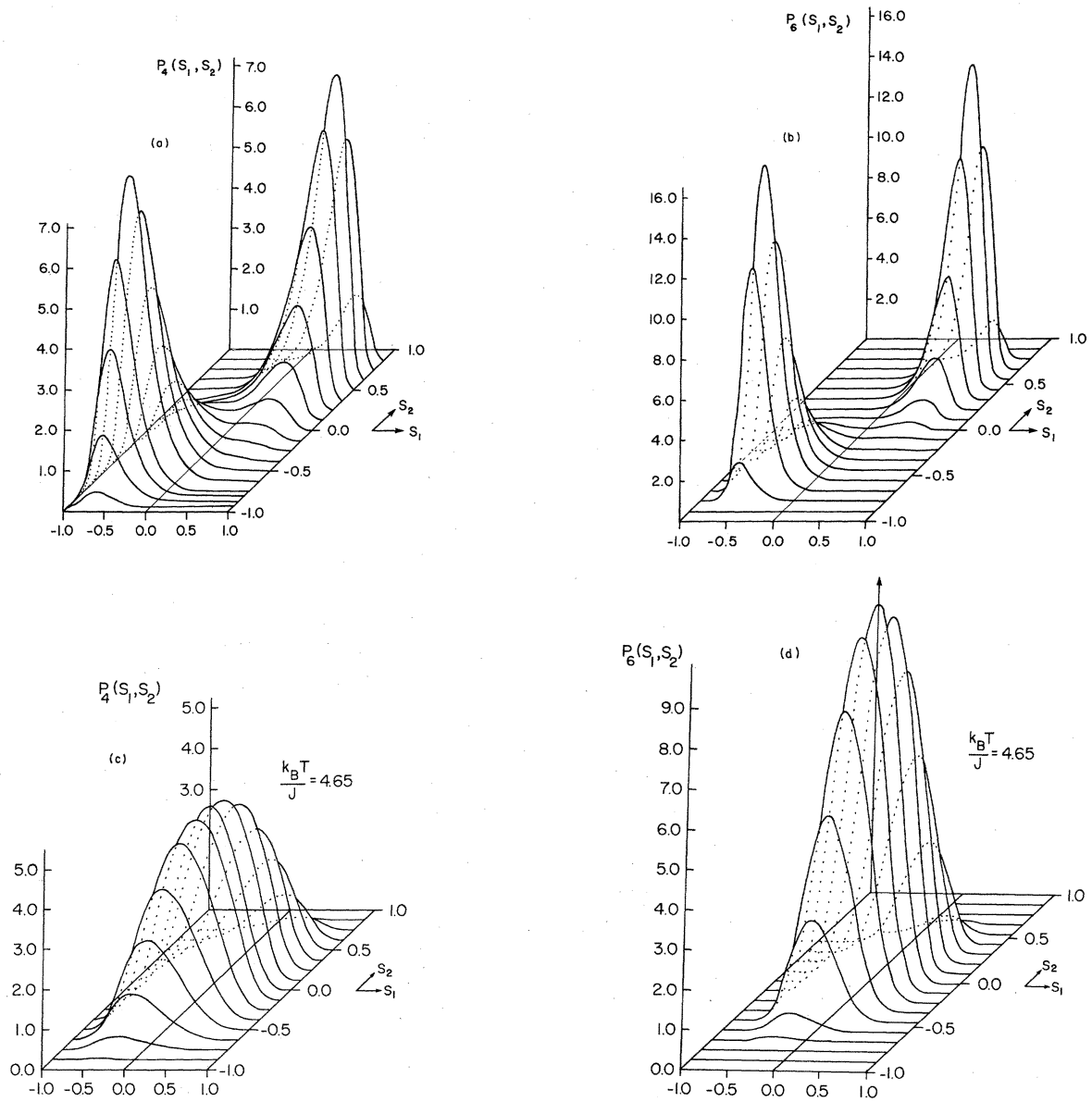

FIG. 3. Joint cell distribution function $P_L(s_1,s_2)$ below and above T_c for linear cell sizes $L=4$ and 6. (a) $L=4$, $k_BT/J=4.4$; (b) $L=6$, $k_BT/J=4.4$; (c) $L=4$, $k_BT/J=4.65$; and (d) $L=6$, $k_BT/J=4.65$.

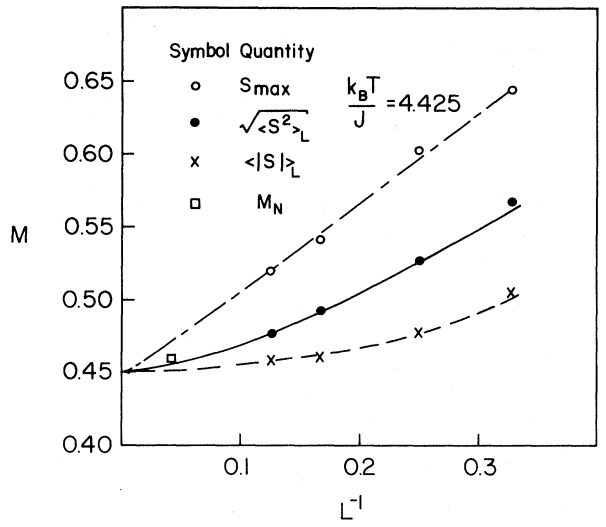

FIG. 4. Estimates of the spontaneous magnetization as obtained from extrapolating from the size dependence of the maximum ($s_{\max}$), the second moment $\langle s^2\rangle_L$ and the first absolute moment $\langle\,|s|\,\rangle_L$ of the joint distribution function.

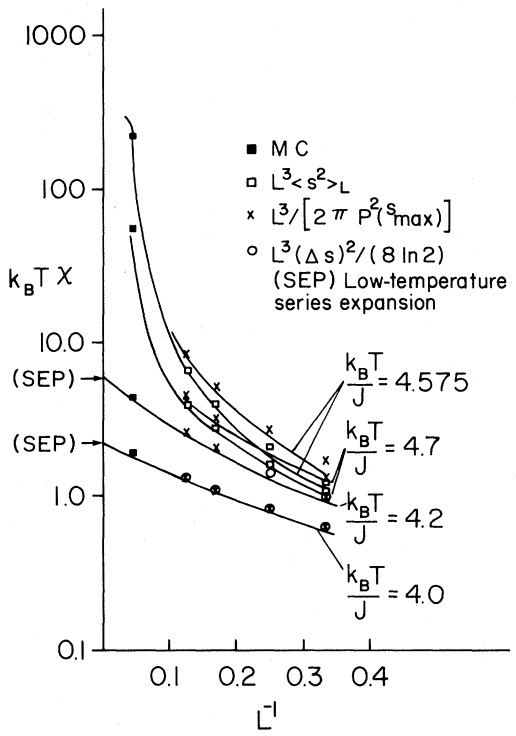

FIG. 5. Various extrapolations of cell observables yielding the susceptibility at several temperatures. Series-expansion results are shown by arrows.

maximum $s_{\max}$ of the distribution function $P_L(s_1,s_2)$. It should be mentioned that we calculated the moments from $P_L(s)$ as well, and the results for $\langle\,|s|\,\rangle_L$ and $\langle s^2\rangle_L$ are the same. This is to be expected due to the simple relationship, (1.6), between these two distribution functions. All three estimates must extrapolate towards the same value, M, for $L\to\infty$. The fact that such extrapolations yield results consistent with each other is an important consistency check on the accuracy of the calculation. It also gives an idea of the finite-size effects below T_c. We note that very close to T_c (or above T_c) $\langle\,|s|\,\rangle_L$ and $\langle s^2\rangle_L$ give spurious nonzero estimates for M due to finite-size effects. In this case $(s_{\max})_L$ will probably yield more reliable results.

Figure 5 shows various estimates of the susceptibility obtained from $P_L(s)$. The validity of these estimates rely on the Gaussian property of $P_L(s)$ for $L\gg\xi$. Above T_c we can use $\langle s^2\rangle_L$, $P_L(s=0)$, or the half-width Δs of the distribution defined as

$$P_L(s_{\max}\pm\tfrac{1}{2}\Delta s)=P_L(s_{\max})/2\ . \tag{3.1}$$

Below T_c one can use P_L $(s_{\max})$ or Δs. These various estimates are consistent with each other and extrapolate to the known series-expansion results for the susceptibility. It should also be mentioned that finite-size effects are large and thus an extrapolation is needed to obtain a reliable estimate of χ. In the neighborhood of the critical temperature ($k_BT_c/J\approx4.51$) the different estimates are inconsistent, showing the breakdown of the Gaussian approximation. This clearly happens at $k_BT/J=4.575$ and can be attributed to the fact that $L\approx\xi$.

In Fig. 6 we show the temperature variation of $P_L(0)$ and $P_L(0,0)$. Since for a sufficiently large cell size both distribution functions must increase with L for $T>T_c$, but decrease with L for $T<T_c$, we can estimate the critical temperature T_c from the intersection of these curves. These estimates are very near but slightly below the series-expansion estimate. Indeed they seem to converge toward the correct T_c.

Next we will check the finite-size scaling assumptions for the single [Eq. (2.5)] and joint [Eq. (2.13)] distribution functions. We have first tested the scaling of $P_L(0)$ and $P_L(0,0)$ above and below T_c. We have chosen[11] $2\beta/\nu=1.03$ and $\nu=0.63$ and plotted $P_L^2(0)L^{-2\beta/\nu}$ and $P_L(0,0)L^{-2\beta/\nu}$ in Figs. 7(a)—7(d). By anticipating a slight shift of the critical temperature due to the finiteness of the system (N^3) causing a ξ/N-dependent correction, we chose $k_BT_c^{\rm eff}/J\approx4.53$, which is less than 0.5% above the series-expansion estimate. The scaling indeed seems to hold since the data points seem to scatter around a single curve, as expected from the scaling hypothesis. Below T_c the scattering is more prominent. This is to be expected since the relative number of Monte Carlo samples is small for $s=s'=0$ as compared to that around the maximum of the distribution functions. For this reason the scaling test above T_c is more reliable than the test below T_c. We have also compared the scaling function for $P_L^2(0)$ with that for $P_L(0,0)$ and found that they are roughly the same, as can be seen from Fig. 7. The similarity of these scaling functions is to be expected on the basis of the discussions in the previous section. We have also made another test of scaling by plotting $(\langle s^2\rangle_L)^{1/2}P_L(s)/2$ vs $s/(\langle s^2\rangle_L)^{1/2}$ and $\langle s^2\rangle_L P_L(s,s)/2$ vs $s^2/\langle s^2\rangle_L$ in Fig. 8. Indeed this test seems to verify scaling. One could also perform the scaling test for the entire function $P_L(s_1,s_2)$, but we have not done this. We instead rely on the two tests above as sufficient indications of scaling.

In Fig. 9 we show the first cumulant versus the inverse

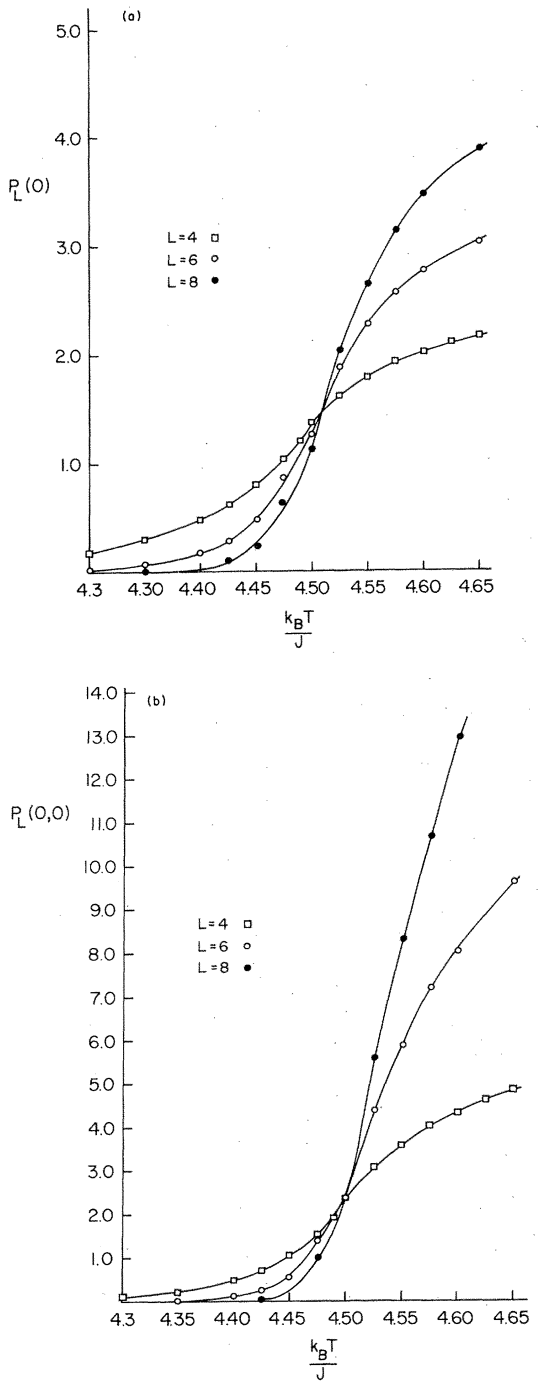

FIG. 6. Temperature variation of (a) $P_L(0)$ and (b) $P_L(0,0)$ for three different linear cell sizes $L=4$, 6, and 8. The critical temperature T_c can be estimated from the crossings of these curves at different cell sizes.

cell size L^{-1}. This plot can be interpreted by analogy with a renormalization-group "flow diagram." Upon change of the length scale three fixed points emerge, as discussed earlier by Binder.[12] $U^*=0$ is the $T=\infty$ fixed point and $U^*=\frac{2}{3}$ is the $T=0$ fixed point. In between (roughly $U^*\approx 0.27$) there is a nontrivial fixed point corresponding to the finite-temperature critical point ($k_BT_c/J=4.525$–4.55). Estimating the critical point from this flow diagram is obviously rather crude. Instead we present a more systematic method to determine the critical behavior by plotting $U_{L'}=U_{L'}(U_L)$. The fixed-point estimate is found when $U_{L'}=U_L=U^*$. If our values of L were large enough, corrections to scaling would be negligible and the estimate U_L^* for U^* should be independent of L. In Fig. 10 we have shown these functions for some pairs of L,L'. These functions are smooth functions throughout the critical region. In particular they could be approximated by straight lines, thus allowing rather accurate estimates of U^*. Our estimates of U^* are somewhat higher than obtained earlier,[12] but are very consistent with each other for different pairs of L and L'. In Fig. 10 we have plotted $U_{L'}/U_L$ as a function of temperature to estimate T_c as obtained from the condition $(U_{L'}/U_L)_{T=T_c}=1$. The values obtained from such condition are within 0.8% of the series-expansion estimate.[17,19] For subsystems of an infinite system, one would expect that the estimates converge to the exact result as L and L' become large. Our best estimate of T_c in fact results from the smallest pair of L and L', however. This may imply that either the convergence is nonmonotonic, or that the effects of the finite linear dimension $N=24$ are still important.[19] We should also note that this way of estimating the critical temperature is independent of any estimates for the critical exponents. We have also estimated critical exponents by a procedure analogous to Nightingale's phenomenological finite-size scaling. Thus we have linearized $U_{L'}=U_{L'}(U_L)$ in the neighborhood of the fixed point U^*:

$$\frac{\partial U_{L'}}{\partial U_L}=\left[\frac{L'}{L}\right]^{(1-\alpha)/\nu}=\left[\frac{L'}{L}\right]^{d-\nu^{-1}}. \tag{3.2}$$

The second equality assumes hyperscaling. Our estimates of the exponent ν are within 5% of the series-expansion conjectures.

We will now summarize the main results of this section. First, from the distribution functions and their moments we were able to obtain reasonable estimates for the magnetization and susceptibility. Second, we were able to show that these distribution functions scale in the vicinity of the critical point. Our value of T_c is roughly consistent with other estimates of T_c. Finally we used finite-size scaling ideas to estimate the critical value for the first cumulant and also obtained a consistent critical point and critical exponents estimates. The estimate of T_c is independent of the estimate of the exponents and vice versa. We have not carried out any finite-size-scaling analysis to correct our estimates of critical behavior because our calculations were limited to rather small cell sizes. For a more accurate study of critical behavior of the Ising model along similar lines, one would have to study a distinctly larger system (allowing larger subsystems) and also improve on the statistics.

IV. PARAMETRIZATION OF THE DISTRIBUTION FUNCTIONS

In this section we will parametrize our numerical data for the single and joint distribution functions in terms of a Ginzburg-Landau–type *Ansatz*. As mentioned in Sec. II such a parametrization can be justified for the total distri-

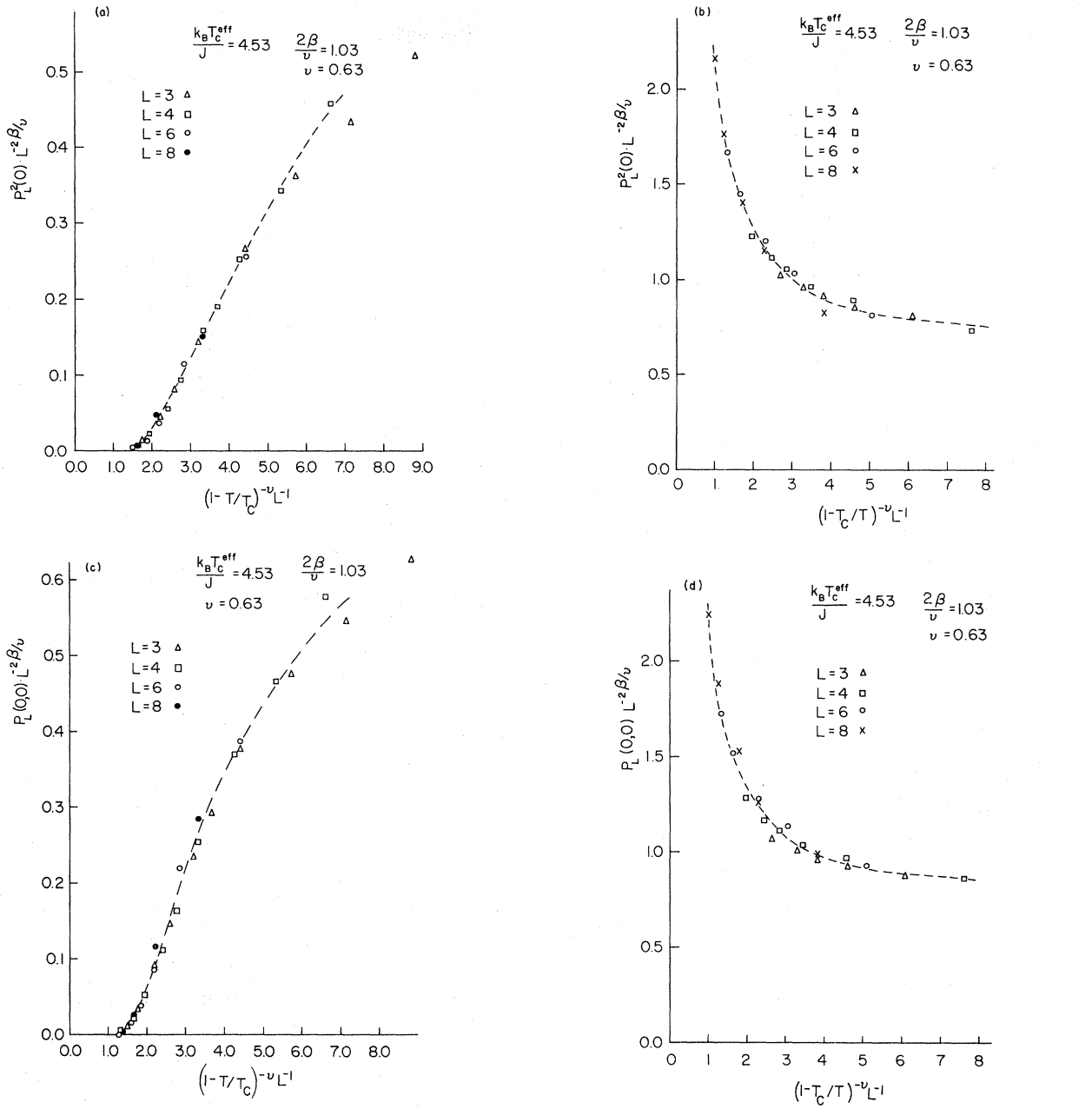

FIG. 7. Finite-size scaling plots of $P_L^2(0)L^{-2\beta/\nu}$ (a) below T_c; (b) above T_c. The scaling plots of $P_L(0,0)L^{-2\beta/\nu}$ (c) below T_c; (d) above T_c.

bution function $P_L(\{s_i\})$. We have carried out the same parametrization for the joint distribution functions $P_L(s_1,s_2)$ and single distribution function $P_L(s)$ and the parameters so obtained show the behavior one might expect.

We have tried two ways to perform this parametrization. The most straightforward way is to make a least-squares analysis to obtain the parameters a_L, r_L, u_L, and c_L in [Eq. (2.17)]

$$-\ln[P_L(s_1,s_2)]=a_L-r_L(s_1^2+s_2^2) +u_L(s_1^4+s_2^4)+c_L(s_1-s_2)^2 . \quad (4.1)$$

For this method to give reliable results one has to weigh the data points in the neighborhood of the peaks of $P_L(s,s')$ (i.e., potential minima) more than the tail parts. This is due to the fact that Monte Carlo procedure samples the peaks much more accurately than the tails; hence the data in the vicinity of the peaks is more reliable. We have not carried out such a detailed analysis. However, we have performed a much simpler, straightforward least-squares analysis without giving different weight to any part of the data. In the second approach we determine the ratios $r_L/2u_L$ and $c_L/2u_L$ of the parameters in Eq (4.1). As is obvious from the discussions of the properties of $P_L(s_1,s_2)$, its maximum occurs at $s_1=s_2=s_{\max}$. Thus it follows from Eq. (4.1) that

$$r_L/2u_L=s_{\max}^2 . \quad (4.2)$$

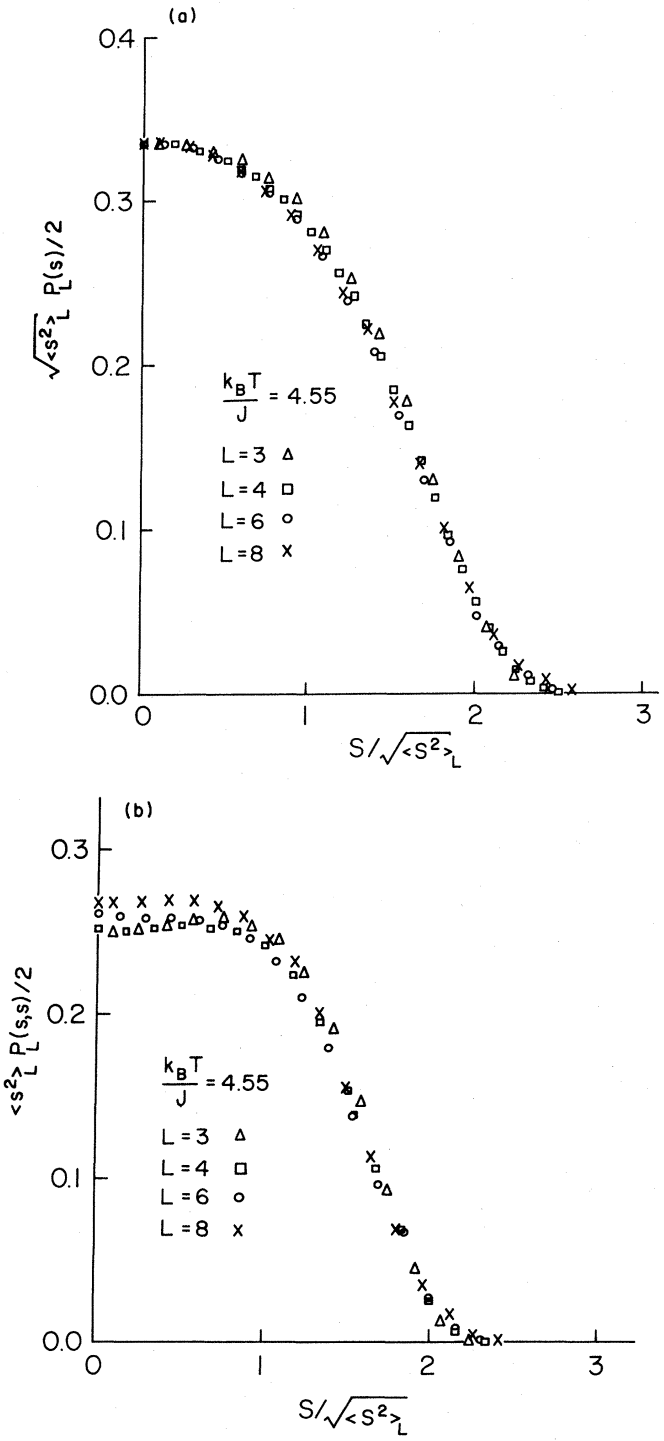

FIG. 8. Scaled cell distribution functions: (a) single distribution and (b) joint distribution functions at the (effective) critical point $k_BT_c/J=4.55$.

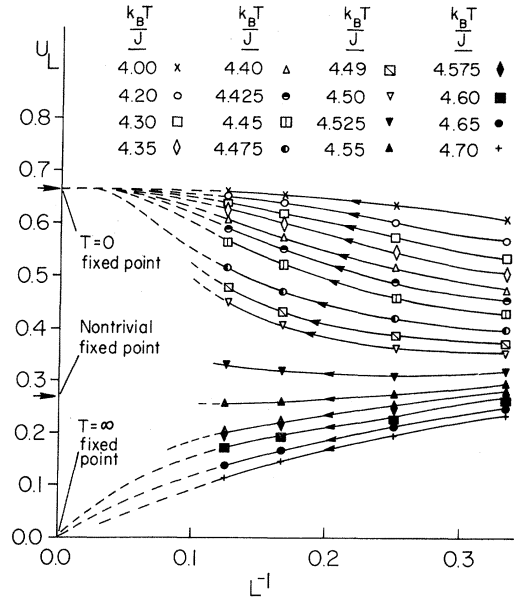

FIG. 9. "Flow diagram" of the first cumulant U_L. Three fixed points are shown. A rough estimate for the nontrivial fixed point value of U can be obtained.

Similarly we can search for a maximum of $P_L(s_1,s_2)$ for fixed s_2 ($\neq s_1$) in the neighborhood of $s_{\max}$. Denoting the maximum of the distribution functions for fixed s_2 by $s_{\max}^{(2)}$ we can write an equation for the gradient term:

$$\frac{c_L}{2u_L} = -\frac{(s_{\max}^{(2)})^3 + s_{\max}^{(2)} s_{\max}}{s_{\max}^{(2)} - s_2} . \tag{4.3}$$

Since above the critical temperature $P_L(s_1,s_2)$ has only one peak at $s_{\max}=0$, Eq. (4.2) can be used only up to the critical temperature. Above T_c we have solved Eq. (4.1) at three different points, $s_1=s_2=0$, $s_1=s_2=s$, and $s_1=s_2=s'$, to determine the quantity $r_L/2u_L$. Alternatively, one could use the least-squares analysis around $s_{\max}=0$. Equation (4.3), however, is valid both below and above T_c. Similarly, one can determine the parameters of the s^4 potential. Then, however, information about the gradient term is lost.

In Fig. 11 we show our results for $r_L/2u_L$ and $c_L/2u_L$ for temperatures both below and above T_c. As is to be expected, $r_L(T)$ changes sign at a temperature $T_c(L)$ which is greater than the bulk critical temperature T_c. We note that our critical-temperature estimates derived in this way also are within 1% of the series-expansion estimate. As well, convergence towards T_c is observed when the cell size is increased. In Fig. 11 we have also shown the M^2 curve as a comparison. The $r_L/2u_L$ curve seemingly converges toward that curve showing only a very small deviation from it for the cell size $L=8$. We have also estimated the critical exponent β from the $r_L/2u_L$ curve below T_c. We obtain results within 5% of the series-expansion estimate $\beta=\frac{5}{16}$. All these results for $r_L/2u_L$ seem to indicate a quantitatively correct estimate for the double-well potential V_L. This also seems to indicate that integrating out degrees of freedom does not strongly affect the shape and parameter values in the double-well potential. We also analyzed the single distribution data in the same way as described above. Quantitatively these results are almost indistinguishable from the results for $P_L(s_1,s_2)$. This further indicates how small a role the gradient term seems to play in changing the parameter ratio $r_L/2u_L$ when one is going from the total distribution function to the joint and single distribution functions, subsequently. As shown in

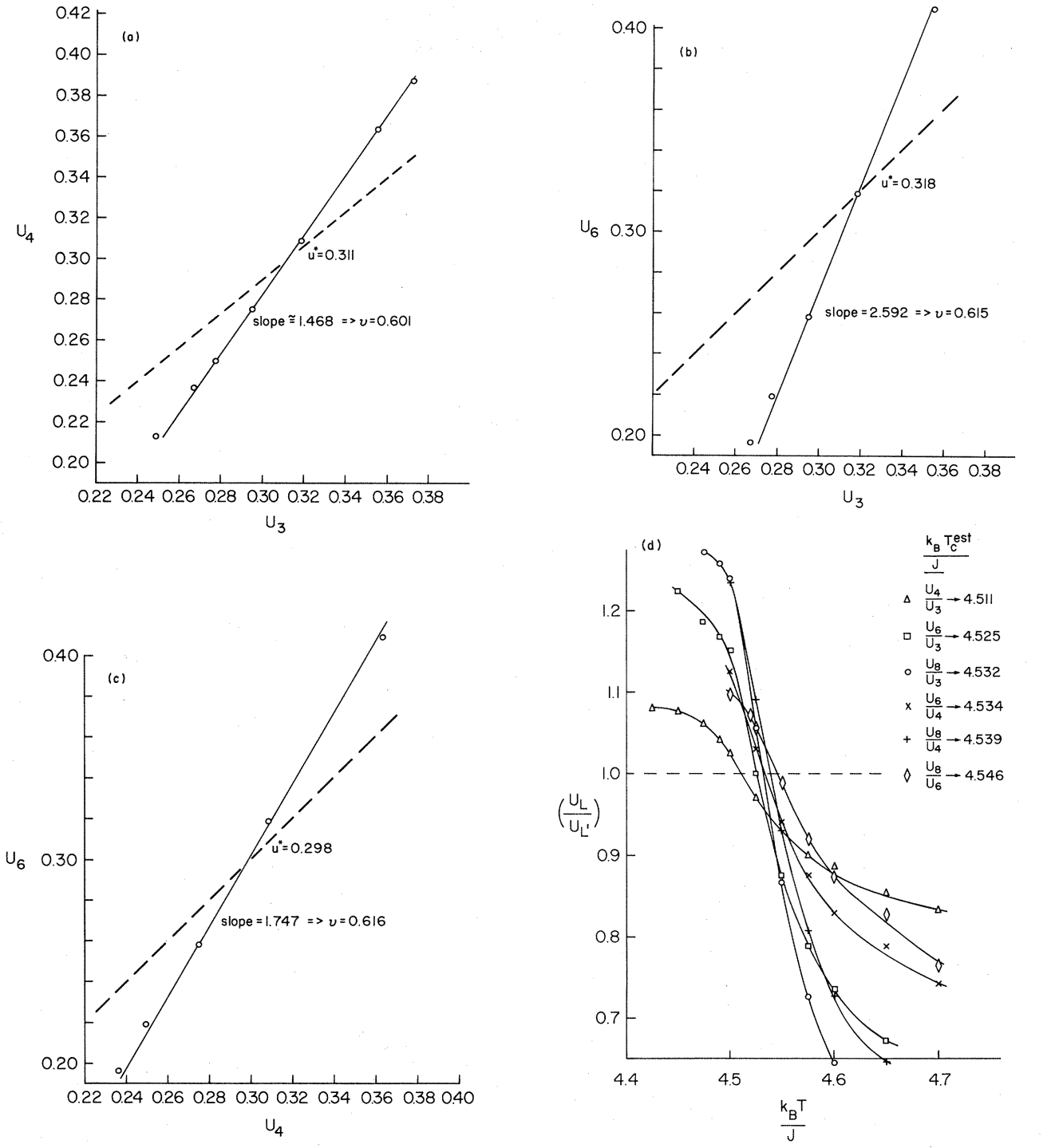

FIG. 10. (a), (b), and (c) $U_{L'}$ plotted as a function of U_L for different choices of L and L'. Fixed point values U^* are given as well as the exponent ν as estimated from the slope. (d) $U_L/U_{L'}$ vs temperature for different pairs of L and L'. Estimates of the critical temperature are shown.

Fig. 11 the ratio $c_L/2u_L$ is only weakly dependent on the temperature for fixed L, as is to be expected. Although the qualitative behavior of c_L seems to be similar to that expected for $\tilde{c}_L$ in (1.4) it is quantitatively not the same as $\tilde{c}_L$. This could be understood from the fact that $P_L(s_1,s_2)$ is a distribution function for *nearest-neighbor* cells. We have also estimated these parameter ratios for a couple of cell sizes and at a few temperatures below T_c using the unweighted least-squares analysis. These results are not inconsistent with those obtained above. Although the overall behavior of the parametrization we have used to study $P_L(s_1,s_2)$ seems to be consistent with the known

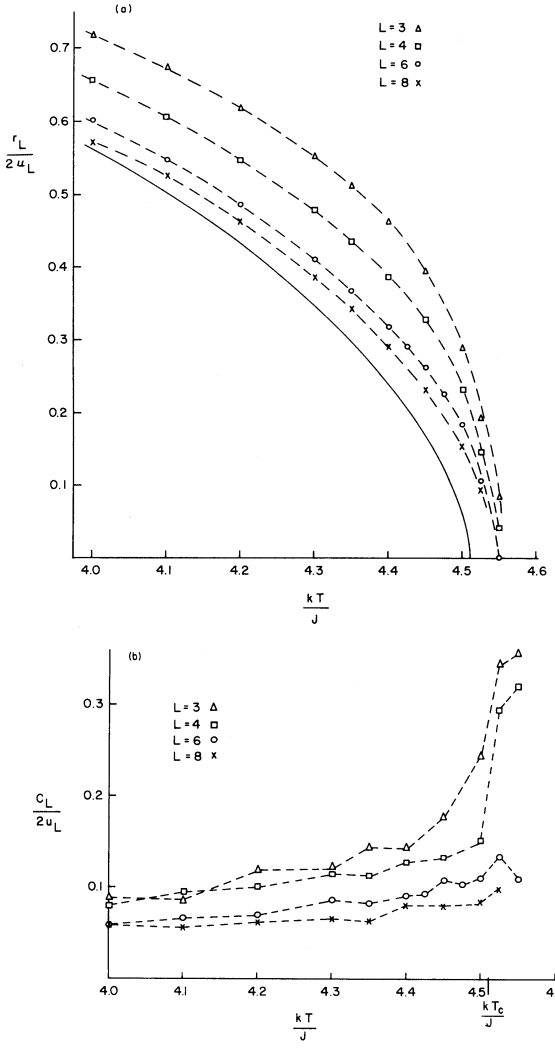

FIG. 11. Parameter ratios (a) $r_L/2u_L$ and (b) $c_L/2u_L$ of Eq. (4.1) vs temperature for cell sizes $L=3$, 4, 6, and 8. The dashed lines are drawn as a visual aid. The square of the spontaneous magnetization is also shown in (a).

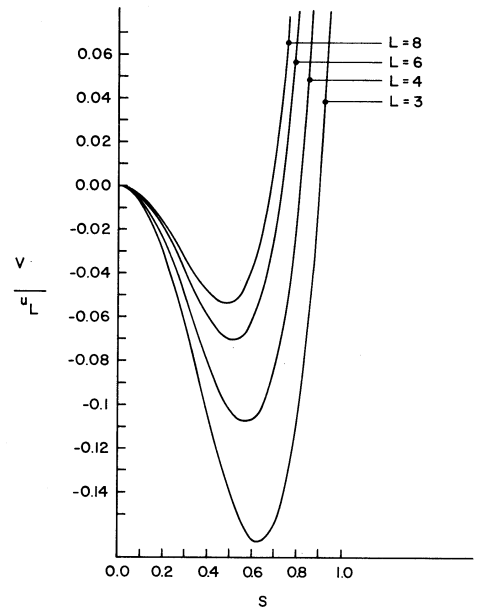

FIG. 12. Potential V_L vs the cell magnetization s at $k_BT/J=4.45$ for linear cell $L=3$, 4, 6, and 8, using the coupling constant $r_L/2u_L$ calculated from $s_{\max}$ of $P_L(s_1,s_2)$.

behavior for the model, these parameters do *not* in general correspond to the parameters in the Helmholtz free-energy functional.

In Fig. 12 we have shown the coarse-grained double-well potential V_L as a function of the cell magnetization s for different cell sizes L, using the parameter ratio $r_L/2u_L$ obtained above. These curves are qualitatively very similar to the coarse-grained double-well potential as determined by a first order in ϵ field-theoretical calculation[3] (where $\epsilon=4-d$ and d denotes the dimensionality).

We now turn to the spinodal curve for the coarse-grained free-energy functional. By analogy with the mean-field theory this could be defined as the function $\tilde{M}_s(L,T)$ for which the second derivative of the coarse-grained free-energy functional with respect to the magnetization vanishes, i.e., $[\partial^2 F_L(M)/\partial M^2]_{T,L}=0$. Although we cannot calculate F_L and hence cannot compute $\tilde{M}_s(L,T)$, we can compute an analogous quantity $M_s(L,T)$ using the definition

$$\left[\frac{\partial^2[\ln P_L(s,s)]}{\partial s^2}\right]_{L,T}=0 \tag{4.4}$$

or

$$\frac{\partial^2[\ln P_L(s)]}{\partial s^2}=0\,. \tag{4.5}$$

We could also estimate $M_s(L,T)$ from the parametrized form (4.1). A more accurate estimate of M_s is to first smooth the $\ln[P_L(s_1,s_2)]$ curve by the method of cubic spline (a standard smoothing routine in most computer libraries) and use the so obtained analytic form to find the zero of the second deriviative. This method is not specifically limited to the s^4 *Ansatz*, as is the parametrized version, (4.1). We would expect that the coarse-grained "spinodal curve" that we have obtained has a qualitatively similar behavior to the curve one would obtain from the Helmholtz free-energy functional. This is based on the rather accurate results which we obtained for the magnetization, susceptibility, and critical behavior in this and the preceding sections. Our results for the "spinodal curve" are given in Fig. 13 in two scaling forms. In this figure we have added the results obtained by Furukawa and Binder[20] for $L/\xi \gg 1$. Their results fit very well with the results of the present study. In Fig. 13(a) the abscissa is $(1-M_s/s_{\max})$ which should approach the Ginzburg-Landau (mean-field) value $(1-1/\sqrt{3})\approx 0.41$ for $(L/\xi)\ll 1$. Our result is within 5% of this limit, in gratifying agreement with theoretical expectations. An alternative scaling form is shown in Fig. 13(b) where the abscissa of Fig. 13(a) is replaced by $(1-M_s/M)$. The magnetization M and correlation length ξ are calculated using the best Padé approximants to low-temperature

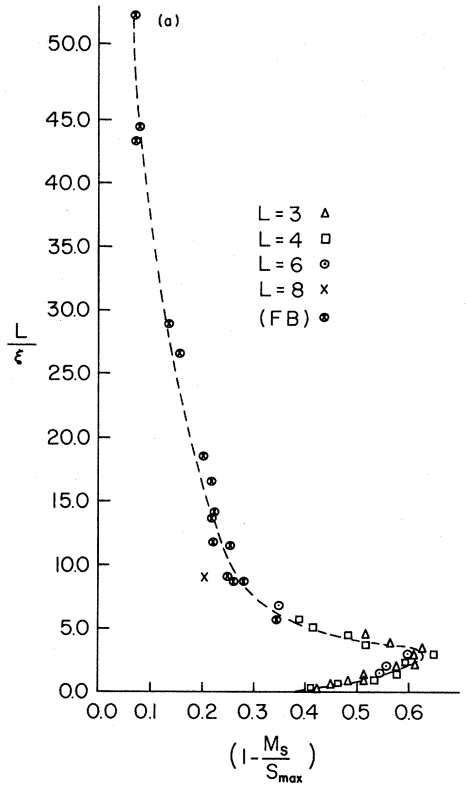

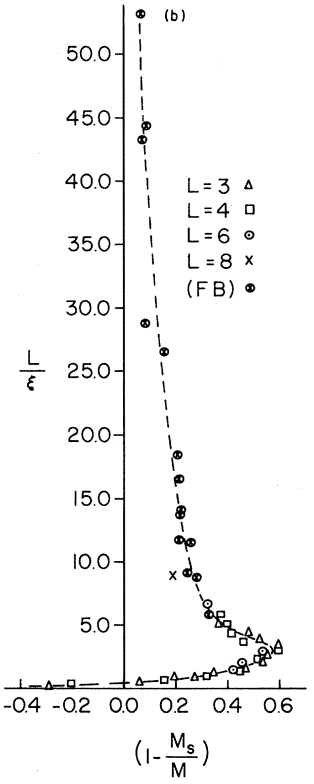

FIG. 13. Two scaling forms of the "spinodal" curve. The magnetization M and correlation length ξ have been calculated using the best Padé approximants of the series expansion, given in Refs. 17 and 18. The dashed lines are drawn as a visual aid.

series expansions.[17,18] With the use of the fact that for $L \ll \xi$ (2.6) implies $\langle s^k \rangle$ to be of the order $L^{-k\beta/\nu}$, together with the heuristic argument that the value M_s taken by s at the spinodal curve should be of the same order as the scale $\langle s^k \rangle^{1/k} \propto L^{-\beta/\nu}$ for the function $P_L(s)$ in this limit, we conclude $M_s \propto L^{-\beta/\nu}$. Since the magnetization itself can be written as $M \propto \xi^{-\beta/\nu}$, we obtain

$$1-\frac{M_s}{M}=1-A(L/\xi)^{-\beta/\nu} \tag{4.6}$$

for $(L/\xi) \ll 1$, where A is a constant. This behavior explains what is seen in Fig. 13(a) for $L/\xi \ll 1$ as well as the change of sign of $(1-M_s/M)$ there.

For $L \gg \xi$ the effective coarse-grained "free energies" $F_L = \ln P_L(s,s)$ or $\ln P_L(s)$ are basically flat for $-M < s < +M$, due to two-phase coexistence, apart from an interface free-energy correction ΔF (see Refs. 14 and 19 for a more detailed discussion). This interface free-energy cost, for a compact region of opposite sign of the order parameter with linear dimension R, in a cell of size L, is of the order of

$$\Delta F \propto (R/\xi)^{d-1}/L^d , \tag{4.7}$$

where we have normalized the free energy per spin. This overturned region leads to a change Δs of the order parameter which is of the order

$$\frac{\Delta s}{M} \propto (R/\xi)^d \tag{4.8}$$

and hence we have

$$\Delta F(\Delta s) \propto (\Delta s/M)^{1-1/d}(\xi/L)\xi^{-d}, \quad R \gg \xi . \tag{4.9}$$

The maximum free-energy enhancement which occurs for $\Delta s \approx M$ is hence of the order ξ/L, when ΔF is measured in units of ξ^{-d}, as should be expected from hyperscaling. Equation (4.8) by itself cannot be used to locate the spinodal, as $\partial(\Delta F)/\partial(\Delta s)$ is monotonically decreasing with Δs, but cannot be used for $\Delta s \to 0$ as there $R \gg \xi$ is no longer fulfilled. To locate the spinodal, we supplement (4.8) with the complementary expansion at the coexistence curve

$$\Delta F(\Delta s) \simeq (\Delta s)^2 \chi^{-1} \propto (\Delta s/M)^2(\xi^{-2\beta-\gamma})^{1/\nu} = (\Delta s/M)^2 \xi^{-d} . \tag{4.10}$$

Matching (4.9) and (4.10) yields the spinodal

$$\frac{\Delta s}{M}=1-\frac{M_s}{M} \propto (\xi/L)^{(1+d^{-1})} . \tag{4.11}$$

We have also analyzed these limiting behaviors, (4.6) and (4.11), for the scaled spinodal curve [Fig. 13(b)] with the use of log-log plots (Fig. 14). Our results for these slopes are consistent with the exponents β/ν and $(1+1/d)$ as referred to in Eqs. (4.6) and (4.11), respectively. It is obvious that these limiting behaviors (4.6) and (4.11) give rise to the turning point at (L/ξ) of order unity. Figure 13(b) show that this occurs for $L/\xi \simeq 3.0$. In contrast to our results a mean-field theory gives a unique thermodynamic spinodal curve. We would expect that a spinodal curve as determined from the coarse-grained Helmholtz free-energy functional would exhibit a qualitatively similar

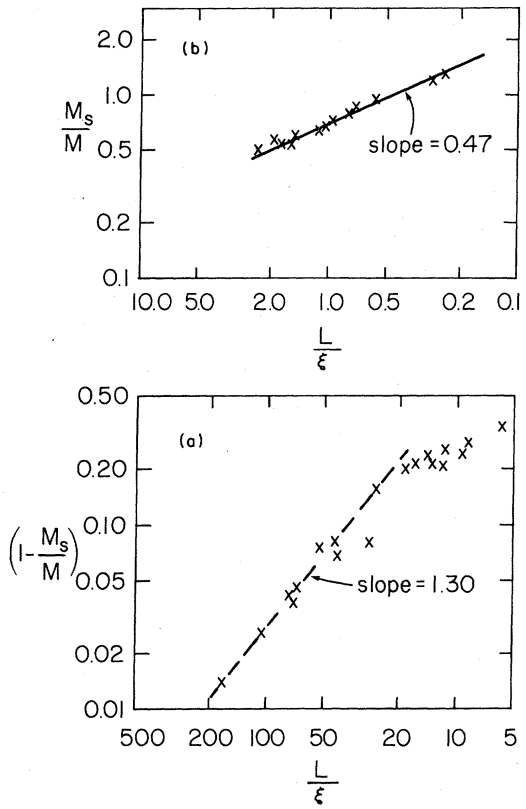

FIG. 14. Limiting behavior of the scaled spinodal curve, Fig. 13(b): (a) $L/\xi \gg 1$; (b) $L/\xi \ll 1$. The slopes are roughly consistent with the expected exponents $1+d^{-1}$ and β/ν, respectively.

behavior to that shown in Fig. 13.

As we mentioned in the Introduction, the coarse-grained Helmholtz free-energy functional is particularly relevant to the theory of spinodal decomposition. This is a process by which a thermodynamically unstable system begins to phase separate. In the most successful nonlinear theory to date,[7] an *ad hoc Ansatz* for F_L was used in the absence of any first-principles knowledge of F_L. Our results as obtained from the joint (or single) distribution function do not yield F_L itself, so we cannot yet test the validity of the *Ansatz*. It should be mentioned, however, that the coarse-grained spinodal curve implicit in this *Ansatz*[7] for $L=(6\pi^2)^{1/3}\xi \simeq 3.9\xi$ differs from our results [Fig. 13(b)] only by an amount $\lesssim 20\%$. Our results also are qualitatively very similar to the field-theoretical calculations of F_L (which are presumably quantitatively inaccurate in three dimensions, since it is only a first order in $\epsilon=4-d$ expansion). Thus our determination of the double-well potential for a coarse-grained system starting from a microscopic model seems a useful step towards developing a continuum theory of the dynamics of phase separation.

V. SUMMARY

In this work we have extended the Monte Carlo "renormalization-group" analysis to study the joint cell distribution function. The results are consistent with the earlier study of single cell distribution functions. We have also obtained some understanding of how a double-well potential, and hence the location of an effective spinodal curve, changes with the coarse-graining size. As noted in the Introduction, however, we have not obtained the Helmholtz free-energy functional. However, we think that our estimates for the parameters r_L and u_L are not too different from the parameters $\tilde{r}_L$ and $\tilde{u}_L$ of the Helmholtz free-energy functional as we have discussed in the text. In contrast it seems clear that our estimated c_L is rather different from the gradient coefficient $\tilde{c}_L$ of the Helmholtz free-energy functional. The reason for this would seem to be the fact that $\tilde{c}_L$ contains information about the long-range correlation of the system while c_L describes only the correlation between nearest-neighbor cells. One might improve the correspondence between $\tilde{c}_L$ and c_L by studying distribution functions for further neighbor-cell separations. As well, one might study the distribution function of a cell and all its nearest neighbors. Alternatively, one might simulate directly the coarse-grained Hamiltonian (1.4) for a variety of values of r_L, u_L, and c_L on a lattice, and determine $P_L(s_i,s_j)$ and $P_L(s_i)$ from such a study. If the resulting distributions can be matched to those obtained in the present work estimates for the parameters r_L, u_L, and c_L describing a nearest-neighbor Ising model would be obtained. This approach seems to us more promising than the possibilities noted above and will be pursued in future work.

ACKNOWLEDGMENTS

This work was supported in part by a grant from the National Science Foundation, No. DMR-80-13700. Two of us (K.K.) and (J.D.G.) wish to acknowledge the kind hospitality of the Kernforschungsanlage, Jülich, where much of this work was performed.

[1]N. G. van Kampen, Phys. Rev. 135, A362 (1964).
[2]L. P. Kadanoff, Ann. Phys. (N.Y.) 2, 263 (1966).
[3]K. Kawasaki, T. Imaeda, and J. D. Gunton, in *Perspectives in Statistical Physics*, edited by H. J. Raveche (North-Holland, Amsterdam, 1981), p. 203.
[4]A. B. Bhatia and N. H. March, J. Chem. Phys. 68, 4651 (1978).
[5]T. Ohta and K. Kawasaki, Prog. Theor. Phys. 58, 467 (1977).
[6]J. Rudnick and D. Jasnow, Phys. Rev. B 17, 1351 (1978).
[7]J. S. Langer, M. Baron, and H. D. Miller, Phys. Rev. A 11, 1417 (1975); see also C. Billotet and K. Binder, Z. Phys. B 32, 195 (1979).
[8]J. D. Gunton, M. San Miguel, and P. Sahni, in *Phase Transitions and Critical Phenomena*, edited by C. Domb and J. L. Lebowitz (Academic, London, 1983), Vol. 8.
[9]K. G. Wilson, Phys. Rev. B 4, 3174 (1971); 4, 3184 (1971).
[10]M. E. Fisher, Rev. Mod. Phys. 46, 587 (1974).
[11]J. C. LeGuillou and J. Zinn-Justin, Phys. Rev. B 21, 3976 (1980).
[12]K. Binder, Z. Phys. B 43, 119 (1981).

[13]B. Chu, J. F. Schoenes, and M. E. Fisher, Phys. Rev. 185, 219 (1969).

[14]K. Binder, Phys. Rev. A 25, 1699 (1982); Phys. Rev. Lett. 47, 693 (1981).

[15]*Monte Carlo Methods in Statistical Physics,* edited by K. Binder (Springer, Berlin, 1979).

[16]C. M. Newman, Commun. Math. Phys. 74, 119 (1980); see also G. A. Baker and S. Krinsky, J. Math. Phys. 18, 590 (1977); J. Jona-Lassino, Nuovo Cimento 26B, 99 (1975).

[17]H. B. Tarko and M. E. Fisher, Phys. Rev. B 11, 1217 (1975).

[18]J. W. Essam and M. E. Fisher, J. Chem. Phys. 38, 802 (1963).

[19]D. Stauffer has performed such a study for systems with $N=40$ and 80, using much larger subsystems in the present work. He finds T_c to within 0.1% of the series expansion value. However, his statistics are not good enough to obtain estimates of the exponents more accurate than those obtained in Ref. 12. [D. Stauffer (private communication)]; see also Fig. 1.3 of the article by K. Binder and D. Stauffer, in Monte Carlo Methods in Statistical Physics II, edited by K. Binder (Springer, Berlin, in press).

[20]H. Furukawa and K. Binder, Phys. Rev. A 26, 556 (1982).